Shearing Interferometer for Quantifying the Coherence of Hard X-Ray Beams
— Source link ⌝

Franz Pfeiffer, Oliver Bunk, Clemens Schulze-Briese, Ana Diaz ...+5 more authors

Institutions: Paul Scherrer Institute, University of Illinois at Urbana–Champaign

Topics: Degree of coherence, Interferometric visibility, Coherence length, Shearing interferometer and Coherence time

Related papers:

- X-ray phase imaging with a grating interferometer.

- Phase retrieval and differential phase-contrast imaging with low-brilliance X-ray sources

- Differential x-ray phase contrast imaging using a shearing interferometer

- Hard-X-ray dark-field imaging using a grating interferometer

- X-ray wavefront analysis and optics characterization with a grating interferometer

Share this paper: 📘 🐦 in ✉

Energy levels of lanthanide ions in a Lu$_2$Si$_2$O$_7$ host

L. Pidol,[1,2] B. Viana,[1] A. Galtayries,[3] and P. Dorenbos[4]

[1]*Laboratoire de Chimie Appliquée de l'Etat Solide, UMR-CNRS 7574, ENSCP, 11 Rue Pierre et Marie Curie,
75231 Paris Cedex 05, France*
[2]*Saint Gobain Cristaux, 104 Route de Larchant, 77140 Saint Pierre les Nemours, France*
[3]*Laboratoire de Physico-Chimie des Surfaces, UMR-CNRS 7045, ENSCP, 11 Rue Pierre et Marie Curie,
75231 Paris Cedex 05, France*
[4]*Faculty of Applied Sciences, Delft University of Technology, Mekelweg 15, 2629 JB Delft, The Netherlands*

Emission and excitation spectra of single crystals of Lu$_2$Si$_2$O$_7$ doped with Ce^{3+}, Pr^{3+}, Nd^{3+}, Sm^{3+}, Eu^{3+}, Tb^{3+}, and Yb^{3+} were measured in the VUV and UV ranges in order to locate the lanthanide energy levels relative to the valence and conduction bands of the matrix. Predictive energy level diagrams for divalent and trivalent lanthanides in Lu$_2$Si$_2$O$_7$ were also constructed thanks to the knowledge of only three parameters. The observed energies of 4f-5d transitions and charge transfer bands are in good agreement with predictions of the level schemes. Finally, as Lu$_2$Si$_2$O$_7$: Ce^{3+} is an efficient scintillator material, these energy diagrams can also be used to go further in the scintillation mechanisms by identifying different traps observed in this scintillator.

PACS number(s): 71.55.−i, 78.55.Hx, 29.40.Mc

I. INTRODUCTION

Performances of many optical materials are determined by the location of lanthanide energy levels relative to the conduction and valence bands of the matrix. Elaboration of a full energy diagram can be very useful for applications, such as phosphors, scintillators or solid-state lasers, as it allows a better understanding of optical behavior.

In this work, we focus on the lanthanide energy levels in the lutetium pyrosilicate (LPS) host. Lu$_2$Si$_2$O$_7$ is a good candidate for such study as it displays only one crystallographic site for the doping lanthanide ion.[1] Furthermore, cerium-doped LPS is a recently developed inorganic scintillator, which displays particularly promising performance for applications such as positron emission tomography (PET) or oil well logging.[2,3] As the scintillation process strongly depends on the location of the excited state or the ground state of the luminescent center relative to the bottom of the conduction band or the top of the valence band, such study is very relevant.

This paper combines a predictive tool, proposed by Dorenbos,[4] and experiments using several spectroscopies. First, the energy levels of each divalent lanthanide relative to the levels of LPS host are obtained by using only three host-dependent parameters. A similar procedure is applied for trivalent lanthanides.[4] Then, these energy level diagrams are compared to new experimental results. Time-resolved spectroscopy in the VUV-range, using synchrotron radiation is employed in this work to study the optical properties of Lu$_2$Si$_2$O$_7$ doped with several lanthanides. The charge transfer phenomena is studied for LPS doped with Sm^{3+}, Eu^{3+}, and Yb^{3+}, whereas one investigates the d-f transitions in Lu$_2$Si$_2$O$_7$ doped with Ce^{3+}, Pr^{3+}, Nd^{3+}, and Tb^{3+}. We have also used x-ray photoelectron spectroscopy (XPS) to establish the relative energy position between the trivalent lanthanide 4f^n level and the valence band. In the last part, the location of lanthanide energy levels is very helpful to understand the scintillation mechanisms. In particular, as thermo-

luminescence (TL) is closely related to the depth of hole or electron traps, the energy level diagram can be very helpful to interpret thermoluminescence glow curves and identify the nature of the different traps.

II. ENERGY LEVEL DIAGRAMS OF DIVALENT AND TRIVALENT LANTHANIDES

First, by using three-parameter model developed by Dorenbos,[4] a predictive energy level scheme of divalent and trivalent lanthanides in Lu$_2$Si$_2$O$_7$ was constructed as shown in Fig. 1. The top of the valence band is defined as the zero of energy. From left to right the level positions of the lanthanides are shown as function of the number of electrons n in the 4f configuration ($n=1$ for Ce^{3+} and La^{2+}, $n=7$ for
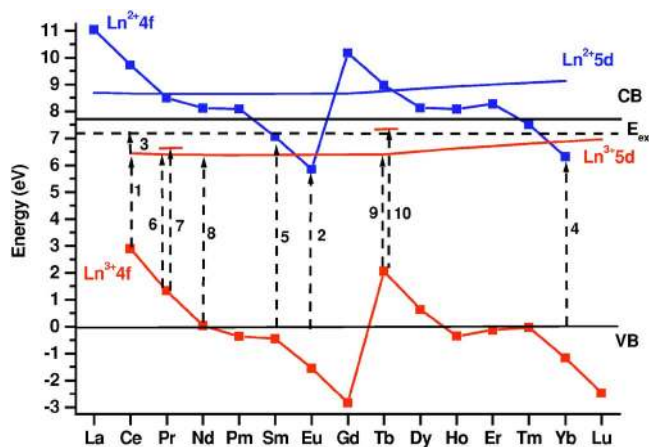

FIG. 1. (Color online) Energy level schemes of divalent (light gray) and trivalent (gray) lanthanides in Lu$_2$Si$_2$O$_7$. The dashed arrows indicate experimental f-d transitions (numbers 1, 6, 7, 8, 9, and 10), charge transfer transitions (2, 4, and 5) and thermal activation energy (3) discussed in the text.
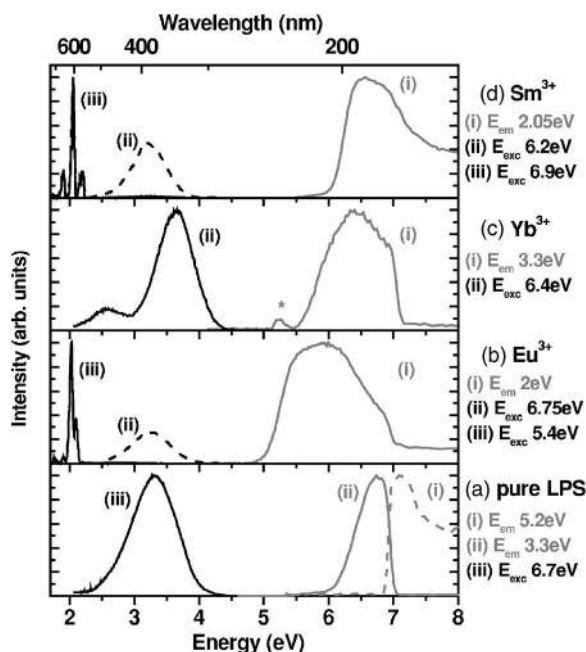
FIG. 2. Excitation spectra (in gray) and emission spectra (in black) at 10 K of (a) pure $Lu_2Si_2O_7$, (b) Eu^{3+}, (c) Yb^{3+}, and (e) Sm^{3+}-doped $Lu_2Si_2O_7$. The corresponding emission and excitation energies, E_{em} and E_{exc}, are given. Peak indicated by a star is attributed to a Tb^{3+}-impurity.

Gd^{3+} and Eu^{2+}, $n = 14$ for Lu^{3+} and Yb^{2+}). The 3-parameter model is based on the knowledge of:[4]

(i) The band gap energy between the top of the valence band and the bottom of the conduction band, which is evaluated to 7.8 eV in the LPS host. The band gap energy corresponds to the creation of a free electron in the conduction band and a free hole in the valence band. The dashed horizontal line (E_{ex}) also presented in Fig. 1 corresponds to the creation of free excitons that can be considered as bound electron hole pairs. This exciton energy is located at 7.15 eV.[5]

The redshift of the fd transition. The redshift is defined as the energy shift of the lowest $5d$ state of a lanthanide with ionic charge Q in a compound (LPS) as compared to the energy of the lanthanide in free space. The redshift of the fd transition is not available for divalent lanthanides in the LPS host. But a good estimation is made from the the redshift value for trivalent lanthanides.[6] One obtains a redshift value of 2.57 eV for $LPS:Ce^{3+}$ from the energy value of 3.55 eV for the first $4f^1 \rightarrow 5d^1$ transition[5] represented by arrow 1 in Fig. 1, and the energy of 6.12 eV for the same transition of free Ce^{3+},[4] and consequently,[6] the redshift of the fd transition is equal to 1.41 eV.

(ii) The energy of charge transfer from the valence band of LPS to Eu^{3+}, which is close to the energy gap between the top of the valence band and the ground state $4f^7$ of Eu^{2+}. The data presented in the following part of the paper [see Fig. 2(b)] lead to a value of 5.85 eV. Arrow 2 in Fig. 1 represents this charge transfer.

The energy differences between the charge transfer to Eu^{3+} and to other trivalent lanthanides do not depend on the host lattice for oxide and fluoride compounds and they are

given by Dorenbos.[4] Consequently, thanks to the charge transfer energy of Eu^{3+} in the LPS host, one may calculate the curve labeled Ln^{2+} $4f$ in Fig. 1, which represents the $4f^{n+1}$ ground states of all divalent lanthanides in LPS host. Then, the redshift for divalent lanthanides permits to determine the energy of the lowest $5d$-level in divalent lanthanides relative to the $4f^{n+1}$-ground state. Combined with the energy of the first $5d$ level for each divalent free lanthanide, it leads to the curve labeled Ln^{2+} $5d$ in Fig. 1, i.e., the first $5d$ level for each divalent lanthanide in LPS host. This means that no d-f emissions are expected for Ln^{2+} ions in LPS host as $5d$-levels are located in the conduction band.

Going deeper in the analysis of the proposed model; the levels for the trivalent lanthanides can be built in the same way.[4] The first two parameters are therefore the band gap energy between the top of the valence band and the bottom of the conduction band and the redshift of the fd transition for trivalent lanthanides in the LPS host, these two parameters being already discussed. A third parameter is also required in order to locate the $4f^n$-ground state or a $4f^{n-1}5d^1$ excited level of one of the Ln^{3+} ions with respect to the valence band or the conduction band. For example, the energy gap between the lanthanide ion ground state and the host conduction band may be obtained by photoconductivity measurements.[7–9] Thermal quenching of Ce^{3+} emission, due to an autoionization process, leads to the energy gap between the first $5d$ excited level and the conduction band.[10] In a previous study about optical properties of Ce^{3+} in LPS host, we have located the first $5d$ excited level at an energy of 0.7 eV below the excitonic level at E^{ex} as sketched in Fig. 1 with arrow 3.[5] From the location of the first $5d$ level of Ce^{3+} the location of the first $5d$ level of the other trivalent lanthanide ions can be estimated. The method can be found in Dorenbos,[4] and the curve labeled Ln^{3+} $5d$ can be constructed. Finally from redshift values, we know the energy differences between the lowest $5d$ state and the $4f$ ground state for each trivalent lanthanide; this leads to the curve labeled Ln^{3+} $4f$ in Fig. 1. As the curve Ln^{3+} $5d$ represents the lowest $4f^{n-1}5d$ level for each Ln^{3+} ion, the transition between the ground state $4f^n$ and this lowest $5d$-level is spin-allowed for Ln^{3+} ions with $n \leq 7$ and it is spin-forbidden with $n \geq 7$.

So, thanks to the 3-parameter model, a full energy level diagram is constructed for all divalent and trivalent lanthanides in the LPS host. This model induces some uncertainties. For instance, on the charge transfer energy of Eu^{3+} one can have a systematic error of about 0.5 eV. Moreover, the energy difference between conduction and valence band, can be modified when the temperature increases, another error could occur. However, the scheme that is constructed by the three-parameter model gives first insights about optical properties and, as we will see later in this paper, it is very useful to interpret spectroscopic results.

III. EXPERIMENT

$Lu_2Si_2O_7$ (LPS), $Er_2Si_2O_7$, $Yb_2Si_2O_7$, and $Sc_2Si_2O_7$ crystals were grown by the melting zone technique. The materials are previously sintered at 1550 °C. For Ln^{3+} doped LPS,

the lanthanide concentrations in the melt are usually 0.5 at %, except for Yb^{3+}(5 at %). $Ce_2Si_2O_7$ was prepared by solid state reaction between CeO_2 and SiO_2, first under reducing atmosphere (Ar/H_2) at 1050 °C and after under argon atmosphere at 1550 °C in a platinum crucible. Samples about 1 mm thick were cut for spectroscopic measurements. For XPS experiments, $Ln_2Si_2O_7$ (Ln=Ce, Er, Yb, Lu, and Sc) materials were ground into fine powder and deposited on a conducting tape. The purity of the phase was checked by x-ray diffraction. $Lu_2Si_2O_7$, $Yb_2Si_2O_7$, and $Sc_2Si_2O_7$ present the thortveitite structure, with monoclinic symmetry space group $C2/m$, whereas $Er_2Si_2O_7$ displays the space group $P2_1/c$.[11] For $Ce_2Si_2O_7$, the high-temperature form was obtained, with the space group $P2_1/c$.[11]

X-ray-excited optical luminescence was generated with an x-ray tube, using a Cu anode, operated at 35 kV and 25 mA. The emission was dispersed with an ARC VM504 monochromator (blazed at 300 nm, 1200 grooves mm^{-1}) and measured with a Hamamatsu R943-02 photomultiplier tube (PMT). Data were corrected for the wavelength dependence of the PMT quantum efficiency and for the monochromator transmission.

High resolution, time-resolved excitation and emission spectra were recorded using synchrotron radiation at the SUPERLUMI station of the Synchrotron Strahlungslabor (HASYLAB) at the Deutsches Elektronen Synchrotron (DESY) in Hamburg, Germany. Emission spectra were recorded with an ARC Spectropro 300I monochromator (blazed at 300 nm, 300 grooves mm^{-1}) and a R6358 Hamamatsu PMT. Excitation spectra were measured on a 2 m normal-incidence McPherson monochromator equipped with two interchangeable holographic gratings (1200 grooves mm^{-1}, blazed at 150 and 300 nm, respectively). The wavelength accuracy was 0.3 nm. Photons were counted with a 13 ns time window at the start of the synchrotron excitation pulse (fast spectrum). Another 81 ns wide time window starting 80 ns after the exciting pulse was used to discriminate between fast and slow luminescence components. The integral count rate was also recorded. Excitation spectra were corrected for the spectral shape of the excitation source by means of Na-salicylate reference measurement. A comprehensive description of both SuperLumi set-up and synchrotron operation characteristics is reported in Ref. 12.

XPS measurements were performed with a VG ESCALAB Mark II X-ray photoelectron spectrometer using an non monochromatized Al K_α anode ($h\nu$=1486.7 eV), at a power of 600 W. Si $2p$, O $1s$, and C $1s$ core level spectra, as well as the region of the valence band (VB), have been systematically recorded at high resolution (pass energy of 20 eV). A survey spectrum was also recorded with a pass energy of 100 eV. A binding energy (E_B) of 284.7 eV was assigned to the C $1s$ peak corresponding to surface contamination (aliphatic carbon) and this was used as an internal reference for correction of charging effects. The satellites due to the nonmonochromaticity of the x-ray source have been subtracted by the satellite subtraction function of the commercial ECLIPSE (VG) program used for data processing. The experimental binding energies are given with an accuracy of 0.1 eV.

The thermoluminescence (TL) glow curves were recorded with a linear heating rate from room temperature to 670 K.

TABLE I. Spectroscopic properties of undoped $Lu_2Si_2O_7$.

	Emission (eV)	Excitation (eV)
STE 1	5.3(FWHM=0.65) at 10 K	Edge followed by maximum at 7.15 eV at 10 K
STE 2	3.35(FWHM=0.7) at 100 K	3.7(FWHM=0.45) at 10 K

Prior to each TL experiment, the crystals (0.5 mm thick) were annealed for several minutes at 670 K. Next, they were exposed during 20 s to β-irradiation ($^{90}Sr/^{90}Y$ source providing a dose of 1 mGray s^{-1} in air). TL glow curves were recorded in N_2 atmosphere with a 0.5 K s^{-1} heating rate, using a TL/OSL system (TL-DA-15) from RISØ.

IV. CHARGE TRANSFER TRANSITIONS

The charge transfer transitions of three ions, Eu^{3+}, Yb^{3+}, and Sm^{3+} are studied here. To distinguish between excitations due to Ln^{3+} charge transfer or due to host lattice absorption, it is necessary to have first a good knowledge about host lattice luminescence and its excitation. Optical properties of pure $Lu_2Si_2O_7$ were already studied and are summarized in Table I.[5,13] Two slow emissions were observed at 5.3 and 3.35 eV that were attributed to self-trapped excitons (STE). They will be referred to as STE 1 and STE 2, respectively. Figure 2(a) shows the 3.35 eV emission in pure LPS. The corresponding excitation spectra consist of an edge followed by a maximum at 7.15 eV. The 5.3 eV emission can be seen in Fig. 4(a). LPS is excited in a broad single band centered at 6.7 eV with a width of 0.45 eV, see Fig. 2(a). The STE1 and STE2 light yields decrease with temperature, due to quenching of STE luminescence.

A. Eu^{3+} charge transfer transition

Excitation spectrum of Eu^{3+}-doped LPS at 10 K, monitoring $4f^6$-$4f^6$ emission at 2 eV is shown in Fig. 2(b) spectrum (i). It can be interpreted as the overlap of two broad bands. The first one is due to the STE2 excitation band which is centered at 6.7 eV with a width of 0.45 eV in pure LPS, see Table I and Fig. 2(a). The more than 1 eV large width of the second one, is characteristic of a charge transfer band, whose average width is 0.91 eV.[4] As the overlap between STE and charge transfer excitation bands is high due to their large widths, it is somewhat delicate to determine exactly the charge transfer energy. We have estimated its value at 5.85 eV. To separate STE and charge transfer excitation bands, Fig. 2(b) shows emission spectra at 10 K for excitation in the high- (6.75 eV) and low- (5.4 eV) energy side of this broad band. Excitation in the STE2-part of the band at 6.75 eV leads to STE2 and $4f^6$-$4f^6$ luminescence, whereas excitation in the CT-part at 5.4 eV gives only $4f^6$-$4f^6$ emission lines [see Fig. 2(b)]. Figure 3(a) presents these $4f^6$-$4f^6$ emission lines of Eu^{3+} excited at 5.4 eV with better resolution thanks to the use of a CCD camera.
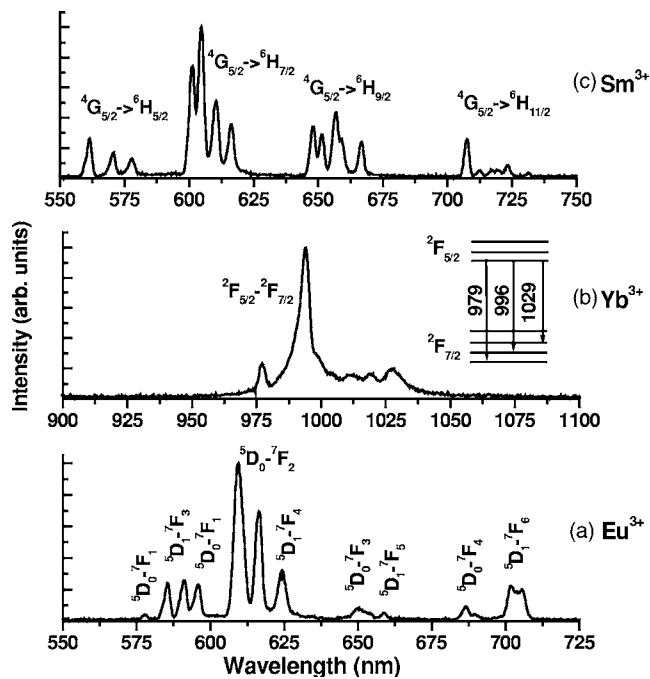
FIG. 3. Emission spectra at 10 K monitoring by CCD camera of (a) Eu^{3+} excited at 5.4 eV, (b) Yb^{3+} excited at 6.2 eV, and (c) Sm^{3+} excited at 6.9 eV in $Lu_2Si_2O_7$ host.

B. Yb^{3+} charge transfer transition

Excitation spectrum for STE1 emission at 3.3 eV in LPS Yb^{3+} is shown in Fig. 2(c) as spectrum (i). It shows an additional broad band around 6.4 eV as compared to the pure compound. By considering the energy diagram in Fig. 1, the charge transfer band of Yb^{3+} in LPS is expected at 6.3 eV. Consequently, the additional broad band is schematized by arrow 4 in Fig. 1. The emission spectrum for excitation at 6.4 eV, which is presented in Fig. 2(c) spectrum (ii), displays two broad bands. The most intense one at 3.65 eV is attributed to the charge transfer transition from the $4f^{14}$ Yb^{2+} ground state to a valence band level. The final state of Yb^{3+} is $4f^{13}(^2F_{7/2})$. The second emission band at 2.55 eV corresponds to the same transition, but with the $4f^{13}(^2F_{5/2})$ level as the final state. The energy separation between the $^2F_{5/2}$ and $^2F_{7/2}$ states of Yb^{3+} is about 1.1 eV, that is close to the theoretical value of 10 000 cm^{-1} (1.25 eV). Figure 3(b) presents $^2F_{5/2}$-$^2F_{7/2}$ emission lines of Yb^{3+} excited at 6.2 eV.

C. Sm^{3+} charge transfer transition

Excitation spectrum of Sm^{3+}-doped LPS at 10 K, monitoring $4f^5$-$4f^5$ emission at 2.05 eV is shown in Fig. 2(d) as spectrum (i). Considering the energy diagrams in Fig. 1, the charge transfer transition of Sm^{3+} in LPS host is expected at 7.05 eV. The low-energy side of the spectrum is attributed to the STE2 excitation band, whereas the high-energy side recalls to the STE1 excitation band in Fig. 2(a). Consequently, the charge transfer transition is strongly overlapped by these two phenomena. We tentatively locate it around 6.95 eV, between the two STE bands. This is schematized by arrow 5 in Fig. 1. Excitation in the low-energy part of the band, at
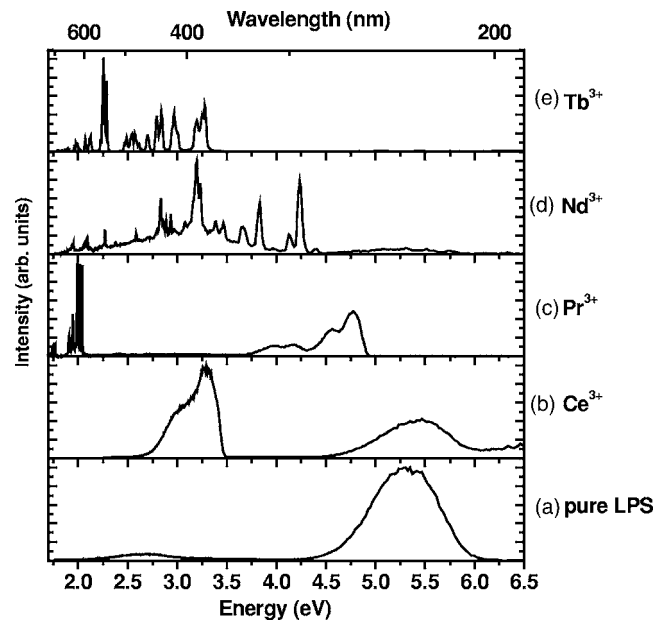

FIG. 4. X-ray-excited luminescence spectra at 100 K of pure $Lu_2Si_2O_7$ (a), Ce^{3+} (b), Pr^{3+} (c), Nd^{3+} (d), and Tb^{3+} (e)-doped $Lu_2Si_2O_7$.

6.2 eV (ii), leads to both STE2 and $4f^5$-$4f^5$ luminescence. Figure 2(d) spectrum (iii) shows that excitation in what is supposed to be the charge transfer band at 6.9 eV gives only Sm^{3+} $4f^5$-$4f^5$ emission. Figure 3(c) presents $4f^5$-$4f^5$ emission lines of Sm^{3+} excited at 6.9 eV measured with the CCD camera.

Up to now, experimental results on the charge transfer transitions for Eu^{3+}, Yb^{3+}, and Sm^{3+} are in good agreement with the predicted energy level positions presented in Fig. 1.

V. f-d TRANSITIONS

After the study of charge transfer transitions, optical properties of other lanthanide ions, such as, Ce^{3+}, Pr^{3+}, Nd^{3+}, and Tb^{3+}, are investigated in order to have information on $4f$-$5d$ transitions.

A. Ce^{3+} f-d transition

The x-ray excited emission spectrum of Ce-doped LPS at 100 K is shown in Fig. 4(b). The broad band at 5.3 eV, also observed in the pure LPS in Fig. 4(a), is attributed to self-trapped exciton emission (STE1). Excitation spectra monitoring this emission lead to the edge at 7.15 eV that can be observed in Fig. 5(a) as spectrum (i) and in Fig. 2(a) as spectrum (i). The Ce^{3+} d-f emission dominates between 2.75 and 3.4 eV. This wide band is due to the allowed transitions from the lowest $5d$-level to the $^2F_{5/2}$ and $^2F_{7/2}$ states of the Ce^{3+} $4f$-configuration at 3.3 and 3.05 eV, respectively. The excitation spectrum of d-f emission at 10 K is presented in Fig. 5(a) spectrum (ii). Four peaks, at 4.15, 5.1, 5.95, and 6.7 eV, are attributed to $4f$-$5d$-excitation bands. Excitation in each of them leads to the same d-f emission, shown in Fig. 5(a) spectrum (iv) where excitation occurs at 4.15 eV.
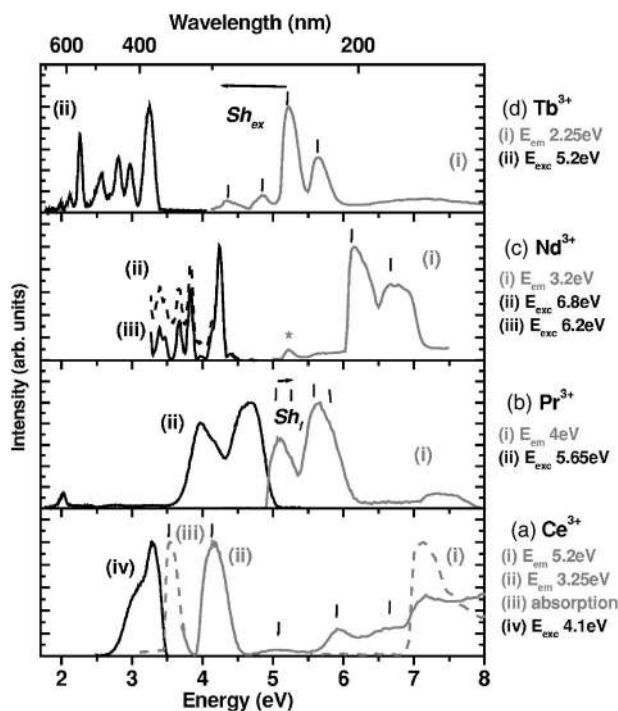
FIG. 5. Excitation and absorption spectra (in gray), emission spectra (in black) at 10 K of (a) Ce^{3+}, (b) Pr^{3+}, (c) Nd^{3+}, and (d) Tb^{3+}-doped $Lu_2Si_2O_7$. The corresponding emission and excitation energies, E_{em} and E_{exc}, are given. Peak indicated by a star is attributed to a Tb^{3+}-impurity. Spin-allowed and spin-forbidden f-d transitions are noticed by vertical bars.

As the Ce^{3+} ion is located in a low C_2-symmetry site, five $5d$-levels are expected. But due to the range limit of the excitation monochromator at 3.71 eV, the lowest $5d$-level can not be observed with the VUV apparatus. However, the optical absorption spectrum of Fig. 5(a) spectrum (iii) locates this peak at 3.55 eV. The five levels are marked by the vertical bars in Fig. 5(a).

B. Pr^{3+} f-d transition

For Pr-doped LPS, the x-ray excited optical luminescence spectrum at 100 K in Fig. 4(c) consists of d-f emission bands between 3.75 and 4.9 eV and $4f^2$-$4f^2$ emission lines between 1.85 and 2.1 eV. The optical excitation spectrum at 10 K monitoring d-f emission at 4 eV is depicted in Fig. 5(b) spectrum (i). The first $4f^2(^3H_4)$-$4f5d$ transition is observed at 5.1 eV, as expected in Fig. 1. The second $4f^2$-$4f5d$ transition is found at 5.65 eV. The splitting of 0.55 eV between the two first $5d$ levels for Pr^{3+} is slightly smaller than the 0.6 eV for Ce^{3+}. Moreover, the width of excitation bands is larger for Pr^{3+} than for Ce^{3+} (FWHM=0.5 and 0.4 eV, respectively). This broadening can be explained by an additional set of $4f5d$ levels at higher energy.[14–17] Indeed, in a simplified model neglecting interaction between f and d electrons, the remaining electron in the $4f$-shell can be found in the $^2F_{5/2}$ or the $^2F_{7/2}$ state. These levels are separated by 0.25 eV for the Ce^{3+} ion. For the $4f^15d^1$ configuration of Pr^{3+}, we estimate a slightly larger spin-orbit splitting, about of 0.3 eV

because of the contraction of the $4f^1$ core after fd excitation.[15] This shift, called Sh_f,[15] is shown in Fig. 5(b). Arrows 6 and 7 in Fig. 1 represent the transitions from the $4f^2$ ground state to the first $4f[^2F_{5/2}]5d$ and $4f[^2F_{7/2}]5d$ levels, respectively. Figure 5(b) spectrum (ii) shows that the excitation in one of the $5d$-level at 5.65 eV leads both to fast d-f emission and slow and weak f-f emission at 2 eV. These two emissions, which are very different in terms of lifetimes, are well separated by the slow and fast spectra monitored with the VUV apparatus. As d-f and f-f emissions are both observed by excitation in $5d$ levels, an energy transfer from $4f^15d^1$ to $4f^2$ levels can occur. That explains the low scintillation efficiency observed for LPS: Pr.[13] Again, this shows the interest of the proposed model to explain the optical properties of the lanthanide doped LPS host.

C. Nd^{3+} f-d transition

The x-ray induced emission spectrum in Fig. 4(d) for LPS:Nd at 100 K presents $4f^3$-$4f^3$ Nd^{3+}-emission lines and a broad emission extending from 2 to 4 eV. The excitation spectrum for f-f emission in the Fig. 5(c) spectrum (i) at 3.2 eV consists of two main bands. From the level scheme of Fig. 1 described in the first part of the paper, the lowest $4f^3$-$4f^25d^1$ transition of Nd^{3+} is expected at 6.35 eV. This corroborates well with the peak at 6.2 eV therefore attributed to this transition, and symbolized by arrow 8 in Fig. 1. The large width of the second band, between 6.5 and 7 eV, can be explained by an overlap between the second $5d$-level and what we called STE 2. Indeed, the splitting of the first two $5d$-levels should be about 0.6 eV. As the first one is situated at 6.2 eV, the second one should appear at 6.8 eV, which is very close to the 6.7 eV excitation band of STE2 emission, see Table I. Moreover, Fig. 5(c) spectrum (iii) shows that excitation at 6.2 eV leads to f-f emission lines only, whereas excitation at 6.8 eV gives f-f emission and an additional slow broad band seen in Fig. 5(c) spectrum (ii). This broad contribution, already observed under x-ray excitation in Fig. 4(d), is attributed to STE2 emission. For Nd^{3+}-doped $Lu_2Si_2O_7$, no d-f emission is observed, due to an efficient nonradiative relaxation from the lowest $4f^25d$ to a $4f^3$ ($^2G_{7/2}$) level, leading to f-f emission.[13,18]

D. Tb^{3+} f-d transition

Finally for the Tb^{3+} ion, spin-forbidden and spin-allowed f-d transitions are usually observed as the excited configuration is $4f^75d^1$. The splitting between the low-spin (LS) and high-spin (HS) fd states is mainly caused by the exchange interaction between the seven aligned spins of $4f$ electrons and spin of the $5d$ electron. Under x-ray excitation at 100 K, only $4f^8$-$4f^8$ emission lines are observed in Fig. 4(e) for Tb-doped LPS. Excitation spectrum monitoring f-f emission at 2.25 eV is shown in Fig. 5(d) spectrum (i). Again, using the predictive model and the scheme of Fig. 1, the first f-d excitation band, which is a spin-forbidden transition, is expected at 4.35 eV. So, the weaker bands at 4.85 and 4.35 eV are attributed to the first two spin-forbidden transitions to the $4f^7[^8S]5d$[HS] levels. In Fig. 1, arrow 9 schematizes the first

spin-forbidden transition; HS indicates a high spin state. The excitation spectra of the Tb:LPS crystal displays two intense bands, which are attributed to $4f^8$-$4f^7 5d$ spin-allowed transitions, i.e., transitions to the $4f^7[^8S]5d$[LS] levels; LS indicates a low spin state. The first one is observed at 5.2 eV and represented by arrow 10 in Fig. 1. The second one is found at 5.7 eV. The splitting between the two first $4f^7[^8S]5d$[LS] levels of Tb^{3+} ion is about 0.5 eV, a comparable value is observed for the first two $4f^7[^8S]5d$[HS] levels. The exchange splitting Sh_{ex} between [HS] and [LS] bands,[15] is presented in Fig. 5(d), and equal to −0.85 eV. This exchange splitting value is close to results obtained for other silicate based materials such as $Y_2Si_2O_7$ or Y_2SiO_5, and therefore corroborates the attribution.[15]

Figure 5(d) spectrum (ii) shows that excitation in the $4f^7 5d$ level at 5.2 eV leads only to slow f-f emission. The d-f emission does not occur due to an efficient multiphonon relaxation from the $4f^7 5d$ level to a $4f^8$ level.

From the experimental data, one observes that the splitting between the first two $5d$ levels slightly decreases from Ce^{3+} to Pr^{3+} and from Pr^{3+} to Tb^{3+} ions (0.6–0.5 eV). The decrease of the crystal field splitting from Ce^{3+} to Tb^{3+} ions in $Lu_2Si_2O_7$ is explained by the decrease of the ionic radius from 1.034 Å for Ce^{3+} to 0.923 Å for Tb^{3+}.[19] Such a result was also reported for YPO_4 and $LiYF_4$.[20,21]

In conclusion, as noticed for the charge transfer transitions, the observed energies of $4f$-$5d$ transitions agree well with predictions of energy diagrams in Fig. 1. Therefore, the energy level schemes built with the three-parameter model appear as very powerful tools to interpret and understand optical properties of all the studied lanthanide cation in the LPS host.

VI. $4f$ BINDING ENERGIES BY XPS

As x-ray photoelectron spectroscopy (XPS) measures the binding energy of both the $4f$ electrons of lanthanide dopants and the upper valence band electrons of the host, one can obtain information on the energy gap between the $4f^n$ level of a trivalent lanthanide and the top of the valence band,[22,23] in the $Lu_2Si_2O_7$ (LPS) host.

Unfortunately, due to a low dopant (<5 at %) concentration in LPS and/or an overlap between the impurity energy bands and host energy bands, XPS measurements on Ln^{3+}-doped LPS does not provide an accurate localization of the lanthanide ion ground state. We have therefore performed XPS measurements on "100% doped" compounds: $Ce_2Si_2O_7$, $Er_2Si_2O_7$, and $Yb_2Si_2O_7$ and results are extrapolated to the corresponding lanthanide-doped $Lu_2Si_2O_7$ host. This approach has been validated by Thiel *et al.* on yttrium aluminum garnet (YAG).[23] They noticed that the $4f$ binding energies are almost identical between lanthanide-doped YAG host (dopant concentration >5 at %) and the corresponding lanthanide aluminum garnet. XPS spectra of the valence band region of $Ce_2Si_2O_7$, $Er_2Si_2O_7$, $Yb_2Si_2O_7$, and $Lu_2Si_2O_7$ are shown in Figs. 6(b)–6(e). The displayed spectra present the $4f$-levels of Ln^{3+}, the $2s$ level of O^{2-}, the $5p$ levels ($5p_{3/2}$ and $5p_{1/2}$) of Ln^{3+} and the $5s$ level is only observed for the Ce-compound.
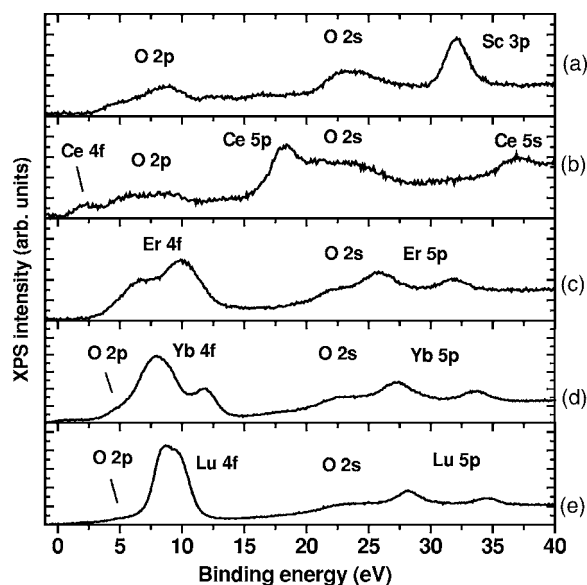

FIG. 6. XPS spectra of the valence band (VB) region of $Sc_2Si_2O_7$ (a), $Ce_2Si_2O_7$ (b), $Er_2Si_2O_7$ (c), $Yb_2Si_2O_7$ (d), and $Lu_2Si_2O_7$ (e).

Since we are interested in measuring the energies of the $4f$-levels with respect to the top of the valence band, we need to determinate the position of the top of the valence band. In the $Lu_2Si_2O_7$ host, the top of the VB is mainly composed by oxygen $2p$-levels, represented by a tail around 5–7 eV in Fig. 6(e). As $4f$-levels of lutetium overlap oxygen $2p$-levels in $Lu_2Si_2O_7$, a direct assignment of the top of the valence band is impossible. Then, attention is focused on Figs. 6(a) and 6(b) on cerium and scandium compounds, where oxygen $2p$-levels are not hidden by the $4f$-levels. As checked with the oxygen $1s$ spectra, not presented here, the binding energies of oxygen levels remain the same for all the studied compounds. By considering oxygen $2p$ levels ($2p_{1/2}$ and $2p_{3/2}$) in scandium and cerium compounds, we have tentatively situated the top of the LPS valence band at 5 eV, which corresponds more or less to the half-width maximum of the first oxygen $2p$-level. This attribution is motivated by results presented in Ref. 23. By calculation, these authors have located the top of the VB near the half-width maximum of the first oxygen $2p$-level. Experimental broadening could lead to an error of 0.5 eV.

The experimental XPS spectra of the $4f$-levels are presented in Figs. 7(a)–7(d). The $4f$ contributions in $Er_2Si_2O_7$, $Yb_2Si_2O_7$, and $Lu_2Si_2O_7$ compounds, are simulated following the method proposed by Thiel.[23] By XPS spectroscopy, an electron is removed from the $4f^n$ level of Ln^{3+}, leading to the corresponding Ln^{4+} ion. This corresponds to transitions between the ground state of the $4f^n$ configuration to the final states of the $4f^{n-1}$ configuration. The energy separation between the different final states are given by the energies of the $4f^{n-1}$ levels of the tetravalent ion, which may be approximated by the well-known level structure of the isoelectronic trivalent ion.[24] As the spin-orbit splitting is larger in tetravalent ion, these values are expanded by 10% to account the enhanced effective nuclear charge.[25] The relative intensity of each level's contribution to the spectrum was estimated using
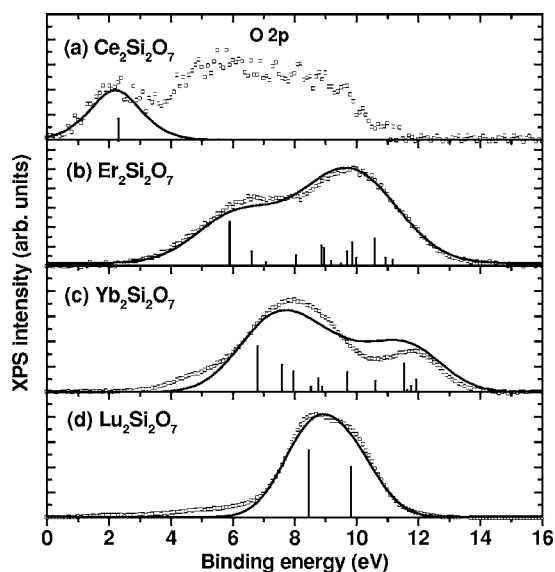
FIG. 7. Experimental XPS spectra of the $4f$ region ($\square$) and calculated spectra obtained from the convolution of Gaussians (solid lines) for $Ce_2Si_2O_7$ (a), $Er_2Si_2O_7$ (b), $Yb_2Si_2O_7$ (c), and $Lu_2Si_2O_7$ (d). Black vertical bars indicate the positions and the relative intensities of each $4f$ final state (see Sec. VI). Only states that contribute more than 0.1% are shown.

FIG. 8. $4f^n$ levels of trivalent lanthanides in $Lu_2Si_2O_7$ obtained by the three-parameter model ($\blacksquare$) and by XPS valence band measurements ($\bigcirc$). For XPS results, the energy corresponds to the energy gap between the $4f^n$ level and the top of the VB (referred to O $2p$ level).

the fractional parentage method reported by Cox.[26] Background removal is performed in Fig. 7 using a Shirley algorithm.[27] All the spectra were convoluted by Gaussian functions. A fairly good agreement is obtained for the three compounds and one can again observe the oxygen $2p$ contribution around $5-7$ eV, which is not taken into account in the calculation (see Fig. 7). These photoemission structures lead to the first $4f$-levels at 2.2, 5.9, 6.8, and 8.5 eV for $Ln_2Si_2O_7$, $Ln=$Ce, Er, Yb, and Lu, respectively. As we have evaluated the top of the valence band at about 5 eV, the energy differences between the $4f^n$ level of trivalent lanthanide and the top of the valence band are calculated.

These energy differences, obtained by XPS, are presented in Fig. 8. They are compared to the predictive three-parameter model presented in the first part of the paper. For lutetium, ytterbium, and erbium, the levels are about 1 eV deeper in the LPS valence band than the ones obtained with the three-parameter model. As energy level diagrams constructed by the three-parameter model use optical spectroscopy results, the deviation between the two methods can be explained by intrinsic differences between XPS and optical spectroscopies. In the photoemission process, electrons are removed to the vacuum after excitation and their kinetic energy is measured, whereas in optical spectroscopy, electronic transitions occur in the optical range. These two methods do not correspond to the same process. Relaxation effects and electronic screening could, for instance, explain the energy difference.[28,29] This systematic error is not observed for the cerium compound, where there is only one $4f$ electron before ionization.

Furthermore, the main difficulty to locate the position of the $4f^n$ levels using photoemission spectroscopy is due to the strong overlap between the host valence band and $4f$-levels
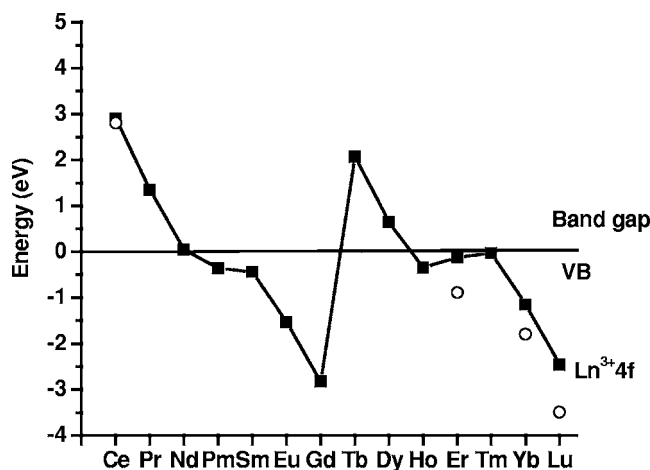
as observed in Figs. 6 and 7. To go in more details in the experimental approach, it would be interesting to employ the technique of resonant photoemission spectroscopy, which gives higher resolution but requires the use of vacuum ultraviolet (VUV) excitation source, using the synchrotron radiation.[23]

VII. ENERGY LEVEL SCHEME APPLIED TO THERMOLUMINESCENCE

The energy gap between the ground state of a divalent lanthanide and the bottom of the conduction band gives information on the possible electron trapping by a trivalent lanthanide ion. In the same way, the energy between the top of the valence band and the ground state of a trivalent lanthanide provides the energy of valence band hole trapping by that lanthanide. As thermoluminescence (TL) is an experimental technique to determine the depth of hole or electron traps, the energy levels scheme, presented in Fig. 1, can be very helpful to analyze TL results.

A typical thermoluminescence glow curve of Ce-doped LPS is presented in Fig. 9(a). Two main peaks appear at 460 K and 520 K. The emission induced by thermal excitation corresponds to the cerium emission. The first hypothesis that can be done is to assign these traps to hole traps, due to Ce^{3+}.[30–34] Using the energy level scheme presented in Fig. 1, Ce^{3+}, Pr^{3+}, and Tb^{3+} ions appear as stable hole traps. Their $4f$-ground states lie, respectively, at 2.9, 1.3, and 2.1 eV above the top of the valence band. Consequently, if Ce^{3+} ion is replaced by Pr^{3+} or Tb^{3+}, the depth of the hole trap should decrease and the glow curve should shift towards lower temperature. As shown in Fig. 9(b), the glow curve of Pr-doped LPS is very similar to that obtained for Ce^{3+} doped LPS. Positions are the same, revealing comparable depths of the traps. Of course, for this ion, the emission induced by thermal excitation is the Pr-one. We may conclude that the two peaks observed by thermoluminescence are not induced by
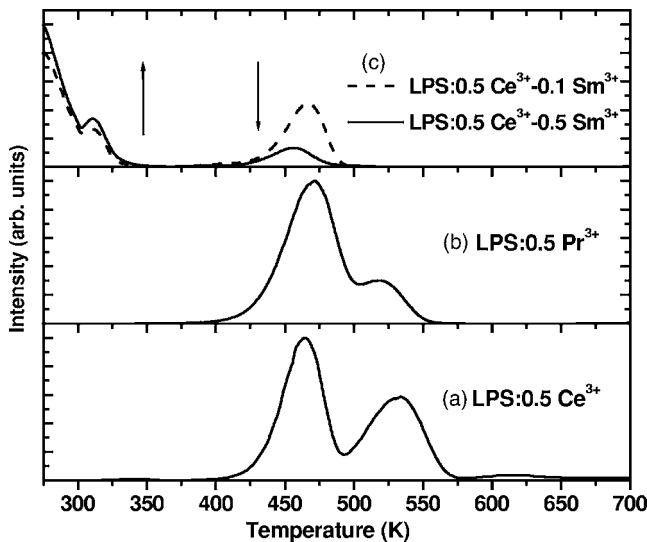
FIG. 9. Thermoluminescence glow curves of LPS crystals (0.5 mm thick), recorded at a heating rate $\beta=0.5$ K s^{-1}, after exposure for 20 s to β-irradiation (^{90}Sr/^{90}Y source, 1 mGray s^{-1}).

thermally activated release of holes from Ce^{4+}, Pr^{4+} or Tb^{4+} ions.

Figure 1 also shows that Ce^{3+}, Pr^{3+}, and Tb^{3+} ions do not trap an electron, since the $4f^{n+1}$ level of the corresponding Ln^{2+} ions is within the conduction band. Ce^{3+}, Pr^{3+} or Tb^{3+} ions, which are stable hole traps, simply act as the recombination center, giving Ce^{3+}, Pr^{3+} or Tb^{3+} emission. The electrons should be trapped by host intrinsic species and the thermal activated release of these electrons determines the TL temperature peak. As reported in the literature,[30,35,36] silicates or other oxides often present oxygen vacancies which act as electron traps.

To confirm this hypothesis, we decided to provide additional electron traps, which compete with the LPS intrinsic ones. From the energy level diagram presented in Fig. 1, Sm^{3+} may act as an electron trap in the LPS host with a depth of 0.7 eV. Experimentally, the addition of Sm^{3+} in LPS:Ce has a marked influence on the glow curve as shown in Fig. 9(c). It shows dominant peaks near room temperature. These latter peaks increase with Sm^{3+} concentration whereas other peaks, characteristics of LPS:Ce, decrease. The peak at 520 K has completely vanished. The $5d$-$4f$ Ce^{3+} emission is mainly observed for all these peaks. This result shows that electrons are trapped by Sm^{3+}, which becomes Sm^{2+},[30,32–34] instead of being trapped by LPS intrinsic defects. As additional TL peaks occur very close to room temperature, these traps are very shallow, in good agreement with Fig. 1 (depth of 0.7 eV). The electron-hole recombination takes place via the Ce^{3+} ion, leading only to Ce^{3+} emission.

VIII. CONCLUSION

By the knowledge of only three parameters, (i) the charge transfer or the activation energy of the thermal quenching, (ii) the redshift, and (iii) the optical band gap, energy level diagrams for divalent and trivalent lanthanides in Lu$_2$Si$_2$O$_7$ host were constructed. Although the level diagrams may contain systematic errors (about 0.5 eV), it provides a consistent interpretation of several spectroscopic features. Optical spectroscopic properties of Lu$_2$Si$_2$O$_7$ doped with several trivalent lanthanide ions were studied. The observed energies of charge transfer bands for Sm^{3+}, Eu^{3+}, and Yb^{3+} ions are in good agreement with predicted energy diagrams. The $4f$-$5d$ transitions of Ce^{3+}, Pr^{3+}, Nd^{3+}, and Tb^{3+} ions, are also well interpreted. Moreover, spectroscopic features of Tb^{3+} and Pr^{3+} were studied in detail, by considering the effect of the isotropic exchange process for Tb^{3+} and the additional transitions due to the f-electron remaining in the $4f^1 5d^1$ excited state of Pr^{3+}.

The valence band region of several lanthanide pyrosilicates has been studied by XPS and the main contributions have been assigned and simulated, leading to the lanthanide $4f$-levels positions. Their energies relative to the top of the LPS valence band, mainly composed of oxygen $2p$-levels, were roughly evaluated as the oxygen $2p$-levels bands are very broad, preventing a precise assignment. Even if a systematic error may occur, the variation in the lanthanide serie is close to the one predicted by the three-parameter model. The slight discrepancy observed for Er, Yb, and Lu-compounds is probably due to intrinsic differences between XPS and optical spectroscopies. To confirm this hypothesis, it will be interesting to study another family of lanthanide-doped compounds.

In this paper, these energy diagrams were also used to have a better understanding of scintillation mechanisms. Thermoluminescence data provides the depth of hole or electron traps. If these traps are due to lanthanide ions, the level schemes can predict the depth values. Thanks to comparison between TL glow curves and energy diagrams, we succeed to identify the traps inside Lu$_2$Si$_2$O$_7$ host during the scintillation process. In conclusion, such energy diagram is a useful tool for many applications of optical materials, such as phosphors, scintillators or solid-state lasers. It is a powerful tool to explain some known behaviors as well as it could predict the properties of unknown compounds.

[1] J. Felsche, Struct. Bonding (Berlin) **13**, 99 (1973).

[2] L. Pidol, A. Kahn-Harari, B. Viana, B. Ferrand, P. Dorenbos, J. T. M. de Haas, C. W. E. van Eijk, and E. Virey, J. Phys.: Condens. Matter **15**, 2091 (2003).

[3] D. Pauwels, B. Viana, A. Kahn-Harari, P. Dorenbos and C. W. E. van Eijk, U.S. Patent No. 6,437,336 (2002).

[4] P. Dorenbos, J. Phys.: Condens. Matter **15**, 8417 (2003).

[5] L. Pidol, B. Viana, A. Kahn-Harari, A. Galtayries, A. Bessiere, and P. Dorenbos, J. Appl. Phys. **95**, 7731 (2004).

[6] P. Dorenbos, J. Phys.: Condens. Matter **15**, 4797 (2003).

[7] M. Raukas, S. A. Basun, W. van Schaik, W. M. Yen, and U. Happek, Appl. Phys. Lett. **69**, 3300 (1996).

[8] W. M. Yen, M. Raukas, S. A. Basun, W. van Schaik, and U. Happek, J. Lumin. **69**, 287 (1996).

[9] C. Pedrini, D. S. McClure, and C. H. Anderson, J. Chem. Phys. **70**, 4959 (1979).

[10] L. J. Lyu and D. S. Hamilton, J. Lumin. **48&49**, 251 (1991).

[11] A. N. Christensen, Z. Kristallogr. **209**, 7 (1994).

[12] G. Zimmer, Nucl. Instrum. Methods Phys. Res. A **308**, 178 (1991).

[13] L. Pidol, B. Viana, A. Kahn-Harari, A. Bessiere, and P. Dorenbos, Nucl. Instrum. Methods Phys. Res. A **537**, 125 (2005).

[14] N. J. M. Le Masson, A. P. Vink, P. Dorenbos, A. J. J. Bos, C. W. E. van Eijk, and J. P. Chaminade, J. Lumin. **101**, 175 (2003).

[15] P. Dorenbos, J. Phys.: Condens. Matter **15**, 6249 (2003).

[16] A. P. Vink, E. van der Kolk, P. Dorenbos, and C. W. E. van Eijk, J. Alloys Compd. **341**, 338 (2002).

[17] M. F. Reid, L. van Pieterson, R. T. Wegh, and A. Meijerink, Phys. Rev. B **62**, 14744 (2000).

[18] R. T. Wegh, W. van Klinken, and A. Meijerink, Phys. Rev. B **64**, 045115 (2001).

[19] R. D. Shannon and C. T. Prewitt, Acta Crystallogr., Sect. B: Struct. Crystallogr. Cryst. Chem. **25**, 925 (1969).

[20] L. van Pieterson, M. F. Reid, R. T. Wegh, S. Soverna, and A. Meijerink, Phys. Rev. B **65**, 045113 (2002).

[21] L. van Pieterson, M. F. Reid, G. W. Burdick, and A. Meijerink, Phys. Rev. B **65**, 045114 (2002).

[22] C. Dujardin, C. Pedrini, J. C. Gâcon, A. G. Petrosyan, A. N. Belsky, and A. N. Vasil'ev, J. Phys.: Condens. Matter **9**, 5229 (1997).

[23] C. W. Thiel, H. Cruguel, H. Wu, Y. Sun, G. J. Lapeyre, R. L. Cone, R. W. Equall, and R. M. Macfarlane, Phys. Rev. B **64**, 085107 (2001).

[24] G. H. Dieke and H. M. Crosswhite, Appl. Opt. **2**, 675 (1963).

[25] J. K. Lang, Y. Baer, and P. A. Cox, J. Phys. F: Met. Phys. **11**, 121 (1981).

[26] P. A. Cox, Struct. Bonding (Berlin) **24**, 59 (1974).

[27] D. A. Shirley, Phys. Rev. B **5**, 4709 (1972).

[28] R. T. Poole, J. Szajman, R. C. G. Leckey, J. G. Jenkin, and J. Liesegang, Phys. Rev. B **12**, 5872 (1975).

[29] R. T. Poole, J. A. Nicholson, J. Liesegang, J. G. Jenkin, and R. C. G. Leckey, Phys. Rev. B **20**, 1733 (1979).

[30] A. Meijerink, W. J. Schipper, and G. Blasse, J. Phys. D **24**, 997 (1991).

[31] D. Meiss, W. Wischert, and S. Kemmler-Sack, Mater. Chem. Phys. **38**, 191 (1994).

[32] K. Chakrabarti, V. K. Mathur, L. A. Thomas, and R. J. Abbundi, J. Appl. Phys. **65**, 2021 (1989).

[33] K. Chakrabarti, V. K. Mathur, J. F. Rhodes, and R. J. Abbundi, J. Appl. Phys. **64**, 1363 (1988).

[34] S. P. Keller, J. E. Mapes, and G. Cheroff, Phys. Rev. **108**, 663 (1957).

[35] D. W. Cooke, B. L. Bennett, R. E. Muenchausen, K. J. McClellan, J. M. Roper, and M. T. Whittaker, J. Appl. Phys. **86**, 5308 (1999).

[36] R. Visser, C. L. Melcher, J. S. Schweitzer, H. Suzuki, and T. A. Tombrello, IEEE Trans. Nucl. Sci. **41**, 689 (1994).